Published OnlineFirst December 23, 2019; DOI: 10.1158/1535-7163.MCT-19-0221

Monoclonal Antibody Targeting Sialyl-di-Lewis^a–Containing Internalizing and Noninternalizing Glycoproteins with Cancer Immunotherapy Development Potential

Silvana T. Tivadar[1], Richard S. McIntosh[1], Jia Xin Chua[2], Robert Moss[1], Tina Parsons[2], Abed M. Zaitoun[3], Srinivasan Madhusudan[1], Lindy G. Durrant[1,2], and Mireille Vankemmelbeke[2]

ABSTRACT

Tumor glycans constitute attractive targets for therapeutic antibodies. The sialylated glycocalyx plays a prominent role in cancer progression and immune evasion. Here, we describe the characterization of the mAb, FG129, which targets tumor-associated sialylated glycan, and demonstrate its potential for multimodal cancer therapy. FG129, obtained through BALB/c mouse immunizations with liposomes containing membrane glycan extracts from the colorectal cancer cell line LS180, is an mIgG1κ that targets sialyl-di-Lewis^a–containing glycoproteins. FG129, as well as its chimeric human IgG1 variant, CH129, binds with nanomolar functional affinity to a range of colorectal, pancreatic, and gastric cancer cell lines. FG129 targets 74% (135/182) of pancreatic, 50% (46/92) of gastric, 36% (100/281) of colorectal, 27% (89/327) of ovarian, and 21% (42/201) of non–small cell lung cancers, by IHC. In our pancreatic cancer cohort, high FG129 glyco-epitope expression was significantly associated with poor prognosis ($P = 0.004$). Crucially, the glyco-epitope displays limited normal tissue distribution, with FG129 binding weakly to a small percentage of cells within gallbladder, ileum, liver, esophagus, pancreas, and thyroid tissues. Owing to glyco-epitope internalization, we validated payload delivery by CH129 through monomethyl auristatin E (MMAE) or maytansinoid (DM1 and DM4) conjugation. All three CH129 drug conjugates killed high-binding colorectal and pancreatic cancer cell lines with (sub)nanomolar potency, coinciding with significant *in vivo* xenograft tumor control by CH129-vcMMAE. CH129, with its restricted normal tissue distribution, avid tumor binding, and efficient payload delivery, is a promising candidate for the treatment of sialyl-di-Lewis^a–expressing solid tumors, as an antibody–drug conjugate or as an alternative cancer immunotherapy modality.

Introduction

Recent advances in cancer cell glycomics have highlighted the differential glycan make-up of tumor cells versus their normal counterparts. During transformation, cancer cells alter their glycosylation profile because of genetic, epigenetic, and metabolic reprogramming of glycosyl transferase activity as well as the availability of nucleotide-glycan donors (1–3). This results in glycan structures with altered branching (N-glycans), truncation due to incomplete synthesis, increased sialylation and fucosylation as well as higher density glycosylation (O-glycans), or altogether novel structures due to neosynthesis (4, 5). This altered glycome affects cancer cell biology, as over 50% of the cellular proteome and a significant fraction of membrane lipids are glycosylated that affects their folding, distribution, and activity (6).

Specifically during cancer progression, altered glycosylation and sialylation of proteins and lipids have profound effects, ranging from immune evasion to increased cellular proliferation and the capacity to metastasize. Immune evasion stems from the interaction of tumor sialoglycans with immune inhibitory sialic acid–binding immunoglobulin-type lectins (siglecs) expressed by innate immune cells, thereby dampening immune cell activation or evading natural killer–mediated killing (7–11). Increased proliferation results from direct and indirect effects on growth factor signaling, and the interaction of sialylated glycans with activated endothelial cell selectins supports cancer cell metastasis (12–14). Oversialylation of a range of human gastrointestinal and pancreatic cancers as well as melanoma has consistently been associated with enhanced proliferative and metastatic potential (15–18).

The original carbohydrate antigen (CA)19.9 was identified via the CA19.9 mAb, obtained through immunizations with the human colon carcinoma cell line SW-1116. CA19.9 is a sialyl-Lewis^a–containing monoganglioside glycolipid that is overexpressed in many gastrointestinal and pancreatic cancers (19, 20). In pancreatic and colon cancer, CA19.9 on secreted mucins is the most consolidated carbohydrate tumor marker, used for early diagnosis as well as for monitoring responses to therapy (21–24).

Here we describe the generation of FG129, a murine (m) IgG1 with kappa light chain, which predominantly targets sialyl-di-Lewis^a–containing glycoproteins. We include extensive evaluation of the FG129-binding specificity as well as its glyco-epitope distribution. On the basis of the favorable FG129 glyco-epitope distribution, we report the creation of a chimeric human (h) IgG1 version, CH129, and demonstrate its potential for payload delivery to target-expressing solid tumors.

[1]Division of Cancer and Stem Cells, School of Medicine, City Hospital Campus, University of Nottingham, Nottingham, United Kingdom. [2]Scancell Limited, University of Nottingham Biodiscovery Institute, Nottingham, United Kingdom. [3]Section of Surgery, School of Medicine, Queens Medical Centre, University of Nottingham, Nottingham, United Kingdom.

Note: Supplementary data for this article are available at Molecular Cancer Therapeutics Online (http://mct.aacrjournals.org/).

Corresponding Author: Lindy G. Durrant, Scancell Limited, University of Nottingham Biodiscovery Insitute, University Park, Nottingham NG7 2RD, United Kingdom. Phone/Fax: 4411-5823-1863; E-mail: lindy.durrant@nottingham.ac.uk

Mol Cancer Ther 2020;19:790–801

doi: 10.1158/1535-7163.MCT-19-0221

Published OnlineFirst December 23, 2019; DOI: 10.1158/1535-7163.MCT-19-0221

Materials and Methods

Materials, cells, and antibodies

All cancer cell lines—gastric (AGS and MKN45), colorectal (COLO205, HCT-15, HT29, LoVo, LS180, DLD1 and SW480), pancreatic (ASPC1 and BxPC3), lung (H69, DMS79 and EKVX), ovarian (OVCAR3, OVCAR4, and OVCA433), breast (DU4475 and MCF-7), as well as the murine myeloma NS0 cell line and normal human umbilical vein endothelial cells (HUVEC)—were purchased from ATCC. All cell lines were authenticated using short tandem repeat profiling. The mAb CA19.9 (ab15146, RRID:AB_301691) was purchased from Abcam, the anti-HLA-ABC (clone W6/32) from eBioscience, and the anti-CD40 from R&D Systems. Incomplete Freund's adjuvant was from Sigma-Aldrich and alpha-galactosylceramide from Alexis Biochemical. Human serum albumin (HSA)–conjugated sialyl-Lewis^a: monosialyl, monofucosyllacto-N-tetraose-APD-HSA was obtained from IsoSepAB.

Generation of mAbs

Plasma membrane lipid extract from 5×10^7 LS180 cells, incorporated into liposomes, was used to immunize BALB/c mice at two-weekly intervals over a 2-month period, with alpha-galactosylceramide and anti-CD40 mAb included as adjuvants. Five days after the final immunization, the splenocytes were harvested and fused with NS0 myeloma cells. Hybridoma supernatant was screened by ELISA and by flow cytometry for LS180 reactivity. Stable clones were established by repeated limiting dilutions and the FG129 mAb was purified from hybridoma supernatant using standard protein G affinity chromatography. mAb isotyping was performed using a standard isotyping kit (Mouse Monoclonal Antibody Isotyping Test Kit, Bio-Rad).

FG129-variable regions' cloning and generation of CH129 (hIgG1) expression construct

Total RNA was prepared from 5×10^6 FG129 hybridoma cells using TRIzol (Invitrogen) following the manufacturer's protocol. First-strand cDNA was prepared from 3 μg of total RNA using a First-Strand cDNA Synthesis Kit and AMV reverse transcriptase following the manufacturer's protocol (Roche Diagnostics). PCR and sequencing of heavy- and light-chain variable regions was performed by Syd Labs, Inc and variable region family usage analyzed using the IMGT database (25). FG129-variable regions were subsequently cloned into the hIgG1/kappa double expression vector pDCOrig-hIgG1 (26) and the sequence confirmed by sequencing.

CH129 HEK293 transfection and mAb purification

The CH129 mAb was obtained following transient transfection of Expi293F cells using the ExpiFectamine 293 Transfection kit (Gibco, Life Technologies). Briefly, HEK293 cells in suspension (100 mL, 2×10^6/mL) were transfected with 100 ng DNA and conditioned medium harvested at day 7 posttransfection. The CH129 mAb was purified using standard protein G affinity chromatography and dialyzed against PBS.

Indirect immunofluorescence and flow cytometry

Cancer cells (1×10^5) or whole blood (50 μL/well) was incubated with primary mAbs (at 33.3 nmol/L) for 1 hour at 4°C, as described previously (27); followed by 1-hour incubation at 4°C with anti-mouse FITC-labeled secondary antibody, lysis of red blood cells (for whole blood binding analysis; Cal-Lyse, Invitrogen), and fixing in 0.4% formaldehyde (Sigma). Cells were run on Beckman Coulter FC-500 and analyzed using WinMDI 2.9. Determination of specific antibody binding capacity (SABC), corresponding to the mean number of accessible antigenic sites per cell was performed using the QiFi kit (Dako) according to the manufacturer's instructions.

Western blot analysis

Cancer cell lysates (from 1×10^5 cells) and total lipid extracts (from 1×10^6 cells) were subjected to SDS-PAGE (4%–12% Bis-Tris, NOVEX, Invitrogen) and transferred to Immobilon-FL PVDF membranes (EMD Millipore). Triplicate samples were loaded and membranes were blocked for 1 hour [5% (w/v) milk in PBS-Tween 20 (0.05% (v/v)] followed by incubation with primary mAbs (7.4 nmol/L) in 2% BSA-PBS-Tween 20 (0.05% (v/v)) overnight at 4°C. Negative control consisted of omission of primary antibody. Secondary antibodies were IRDye 800CW donkey anti-mouse or IRDye 800CW goat anti-human (LI-COR Biosciences), both used at 1:5,000 for 1 hour at room temperature. mAb binding was visualized using a LI-COR Odyssey scanner.

Lewis antigen and sandwich ELISA

ELISA plates were coated with 100 ng/well Lewis-HSA antigens (direct ELISA) or 200 ng/well FG129/CH129 (for sandwich ELISA), blocked with 2% (w/v) BSA-PBS, followed by incubation with primary mAb (direct ELISA) or sera from healthy donors, patients with pancreatic cancer, or mouse serum from a COLO205 xenograft model (sandwich ELISA). Bound antibody (direct ELISA) was detected using streptavidin-HRPO (Thermo Fisher Scientific); bound antigen (sandwich ELISA) was detected using in-house biotinylated-FG129 and streptavidin-HRPO. Plates were read at 450 nm on a Tecan Infinite F50.

Glycan array analysis

FG129 was screened by the Consortium for Functional Glycomics (CFG) for binding to ≥600 natural and synthetic glycans (core H group, version 5.1). Briefly, slides were incubated with 300 nmol/L FG129 for 1 hour, before detection with Alexa Fluor 488–conjugated secondary mAb.

Affinity determination

The kinetic parameters of FG129 and CH129 binding to sialyl-Lewis^a-APD-HSA (sialyl-di-Lewis^a is not commercially available) were determined by surface plasmon resonance (SPR; Biacore 3000, GE Healthcare). Increasing concentrations (0.3 nmol/L–200 nmol/L) of FG129 and CH129 were injected across a sialyl-Lewis^a-APD-HSA–coupled CM5 chip and binding data fitted, using BIA evaluation 4.1. The chip contained four cells, two of which, HSA-coated (in-line reference cells), the other two were coated with low [30 response units (RU)] and high amounts (360 RU) of sialyl-Lewis^a-APD-HSA, mimicking cell surfaces with low and high glyco-epitope expression.

IHC

Tumor and normal tissue binding was assessed on tissue microarrays (TMA) as described previously (27). In brief, after antigen retrieval and blocking of endogenous peroxidase activity and nonspecific binding sites, the slides were incubated with FG129 (7.4 nmol/L) at room temperature for 1 hour, followed by detection with a biotinylated secondary mAb (Vector Laboratories). The slides were subsequently incubated with preformed streptavidin/biotin-HRPO (Dako Ltd.) and 3,3′-diaminobenzidine and finally counterstained with hematoxylin. Staining was scored by two independent assessors, using New Viewer software 2010. The sections were given a semiquantitative histologic score (H-score, 0–300) based on the cellular staining

Published OnlineFirst December 23, 2019; DOI: 10.1158/1535-7163.MCT-19-0221

intensity: negative (0), weak (1), moderate (2), and strong (3) and on the percentage of positive cells. Stratification cut-off points for the survival analysis (SPSS 13.0, SPSS Inc) were analyzed using X-Tile software (28). P values < 0.05 were considered significant.

Patient cohorts

The study populations included cohorts from the consecutive series of 462 archived colorectal cancer specimens (1994–2000; median follow up 42 months; censored December 2003; ref. 29); patients with lymph node–positive disease routinely received adjuvant chemotherapy with 5-flurouracil/folinic acid), 350 ovarian cancer samples (1982–1997; median follow-up 192 months; censored November 2005; patients with stage II to IV disease received standard adjuvant chemotherapy, which in later years was platinum based; ref. 30), 142 gastric cancer samples (2001–2006; median follow up 66 months; censored Jan 2009; no chemotherapy; ref. 31), 68 pancreatic and 120 biliary/ampullary cancer samples (1993–2010; median 45 months; censored 2012; 25–46% of patients received adjuvant chemotherapy with 5-fluorouracil/folinic acid and gemcitabine; ref. 32), and 220 NSCLC (January 1996–July 2006: median follow up 36 months; censored May 2013; none of the patients received chemotherapy prior to surgery but 11 patients received radiotherapy and 9 patients received at least 1 cycle of adjuvant chemotherapy postsurgery) obtained from patients undergoing elective surgical resection of a histologically proven cancer at Nottingham University Hospital (Nottingham, United Kingdom) or Derby University Hospitals (Dery, United Kingdom). No cases were excluded, unless the relevant clinicopathologic material/data were unavailable. Studies involving human participants were approved by the Nottingham Research Ethics Committee and were in accordance with the 1964 Helsinki declaration and its later amendments or comparable ethical standards. Written consent was obtained from all participants.

Competition flow cytometry–based cell binding assay

AlexaFluor 488–labeled [according to the manufacturer's protocol (Invitrogen) FG129, 66.7 nmol/L] was preincubated for 1 hour at 37°C with 100 μL of undiluted serum from patients with pancreatic cancer or healthy human volunteers. Subsequently, cell binding to prefixed (1% formaldehyde) HCT-15 (1×10^5 cells) was analyzed on a Beckman Coulter FC-500 (WinMDI 2.9).

Confocal microscopy

AlexaFluor 488 (495/519nm)-labeled FG129 was added to 1.5×10^5 cancer cells on glass coverslips and incubated for 1 hour at 37°C. During the last 30 minutes of the incubation, Hoechst 33258 (350/461 nm) nucleic acid stain (1 μg/mL), and LysoTracker deep red (647/668 nm) lysosomal stain (50 nmol/L), and CellMask Orange (554/567nm) plasma membrane stain were added to the cells (Invitrogen). Cells were imaged with a ZEISS LSM 510 ConfoCor II confocal microscope (63× 1.4 NA oil objective) and LSM Image Browser was used for image processing.

mAb internalization and payload delivery assay

Payload delivery by FG129 was initially evaluated by measuring the cytotoxicity of immune-complexed FG129 with a saporin-conjugated anti-mouse or anti-human (33). Fab-ZAP secondary conjugate (Advanced Targeting Systems; ref. 33). Target cells were plated overnight in triplicate into 96-well plates (2×10^3 cells, 90 μL/well). After preincubation (30 minutes at ambient temperature) with a concentration range of FG129 and 50 ng of the Fab–ZAP conjugate, 10 μL of conjugate or free FG129 were added to the wells and incubated for 72 hours. Control wells, consisted of cells incubated without conjugate, incubated with secondary Fab-ZAP without primary mAb and incubated with a control mAb preincubated with Fab-ZAP. Cell viability was measured by ^{3}H-thymidine incorporation during the final 24 hours. Normalized results are expressed as a percentage of cells incubated with primary mAb only (control).

Drug conjugation

The following payload and linker chemistries were used for CH129: (i) auristatin monomethyl auristatin E (MMAE) linked via a cleavable dipeptide valine-citrulline (vc) linker, CH129-vc-MMAE, including a para-aminobenzylalcohol (PABA) self-immolative spacer; (ii) maytansinoid emtansine, DM1, via the noncleavable linker succinimidyl 4-(N-maleimidomethyl)cyclohexane-1-carboxylate) (SMCC); and (iii) maytansinoid DM4 via the hindered disulphide linker succinimidyl 3-(2-pyridyldithio)propionate (SPDP) CH129-DM4, which is intermediately cleavable. Direct payload conjugation, via reduced interchain disulfides, was performed by ADC Biotechnology Ltd. Briefly, Tris (2-carboxy-ethyl)-phosphin-HC–reduced CH129 (formulated at 2.3 mg/mL in PBS) was pH-adjusted to approximately pH 7.5. The antibody was then conjugated to MMAE by the addition of five molar equivalents of vc MMAE (60 minutes). CH129 conjugation to DM1-MCC and DM4-SPDP occurred in a similar manner, at 10 molar equivalents relative to the mAb (2 hours). Conjugates were purified on a G25 desalting column. A matched set of control (non-targeting) rituximab (10 mg/mL in pH 6.5 citrate buffer)-based antibody–drug conjugate (ADC) constructs was also produced. The drug-to-antibody ratios (DAR) were determined following size-exclusion chromatography (SEC) in the case of MMAE conjugates and by hydrophobic interaction chromatography (HIC) for the DM1 and DM4 conjugates (Supplementary Table S1).

In vitro ADC cytotoxicity

The cytotoxic effect of the CH129-ADC or control RTX-ADC constructs was assessed using the water-soluble tetrazolium salt WST-8 (CCK8 kit, Sigma-Aldrich). Briefly, after overnight plating of cancer cells (2×10^3 cells/well), the ADC constructs were added at different concentrations in a final volume of 10 μL/well, and the plates incubated at 37°C (5% CO_2) for 72 hours. WST-8 reagent was added (10 μL/well) followed by a further 3-hour incubation after which the OD 450nm was determined (Tecan Infinite F50) and the surviving fraction calculated. EC_{50} values were determined using nonlinear regression (GraphPad Prism v 5).

In vivo ADC tumor control in COLO205 xenograft model

The study was conducted by CrownBio UK under a UK Home Office Licence in accordance with NCRI, LASA, and FELAS guidelines. Animal welfare for this study complies with the UK Animals Scientific Procedures Act 1986 (ASPA) in line with Directive 2010/63/EU of the European Parliament and the Council of September 22, 2010 on the protection of animals used for scientific purposes. Subcutaneous tumors of a human colorectal adenocarcinoma model of COLO205 were established in age-matched female BALB/c nude (Charles River) mice via injection of 5×10^6 viable cells in 0.1 mL serum-free RPMI: Matrigel (1:1) into the left flank of each mouse. Mice ($n = 10$) were randomly allocated to treatment groups based on their tumor volume (mean tumor volume per group at start of dosing: 63.2 $mm^3 \pm 3.9$ mm^3, study day 7) and dosed intravenously (i.v.), biweekly, with 0.1 mg CH129-ADC or RTX-ADC (control) or vehicle (PBS, 100 μL) for a total of four doses. Tumor growth was monitored up until week 4. Body weight and tumor volume were assessed three times weekly and

reduction in tumor volume analyzed statistically using a two-way ANOVA test with Bonferroni posttest (interaction factors; GraphPad Prism v 7.4, GraphPad Inc).

Results

FG129 as well as chimeric hIgG1, CH129, recognize their sialyl-di-Lewis^a glyco-epitope on glycoproteins from a range of cancer cell lines

FG129 is a mouse IgG1 with kappa light chain (Supplementary Fig. S6). Variable region sequencing demonstrated that the FG129 heavy chain belongs to the mouse heavy chain IGHV10-1*02 (IGHD1-1*01, IGHJ4*01) family with three mutations compared with the parental germline sequence. The FG129 light chain belongs to the mouse kappa chain IGKV8-19*01 (IGKJ4*01) family with two mutations compared with the parental germline sequence.

Glycan array (CFG) analysis of the FG129 glyco-epitope binding profile revealed a high specificity of FG129 for sialyl-di-Lewis^a (100%) as well as the two closely related glycans, sialyl-Lewis^a-Lewis^x (89%) and sialyl-Lewis^a (89%), the latter only when presented on a long carbon spacer (eight carbons, sp8; **Fig. 1A**; Supplementary Table S2 and http://www.functionalglycomics.org/glycomics/HServlet?operation=view&sideMenu=no&psId=primscreen_6165). FG129 did not bind the closely related, dietary-derived, N-glycolylneuraminic acid (Neu5Gc)-Lewis^a, nor did it bind unsialylated Lewis^a, Lewis^x, sialyl-Lewis^c, or sialyl-Lewis^x, indicating that its specificity is largely driven by terminal and accessible sialyl-Lewis^a recognition. In addition, the recognition was specific for sialic acid in alpha 2–3 linkage as no binding to alpha 2–6 or alpha 2–8 sialylated glycoconjugates was detected.

The overall cancer cell surface binding by FG129 was analyzed using flow cytometry. FG129 showed strong cell surface binding [geometric mean (Gm) $\geq$1,000] to colorectal tumor cell lines such as HCT-15 and COLO205, somewhat lower to pancreatic lines such as ASPC1 and BxPC3; moderate binding (Gm ~100–1,000) to LS180, DLD1, MKN45, DMS79, and H69 and low binding (Gm < 100) to HT29. FG129 displayed negligible binding to AGS, SW480, EKVX, MCF-7, LoVo, DU4475, OVCAR3, OVCAR4, and OVCA433 (**Fig. 1B**; Supplementary Fig. S1A). Quantitative analysis of the antibody-binding capacity (ABC) on a subset of the high- to moderate-binding cell lines revealed 6.2 $\times$ 10^5 antigenic sites for COLO205 compared with 2.2 $\times$ 10^5 for HCT-15 and approximately 1.2 $\times$ 10^5 for both BxPC3 and

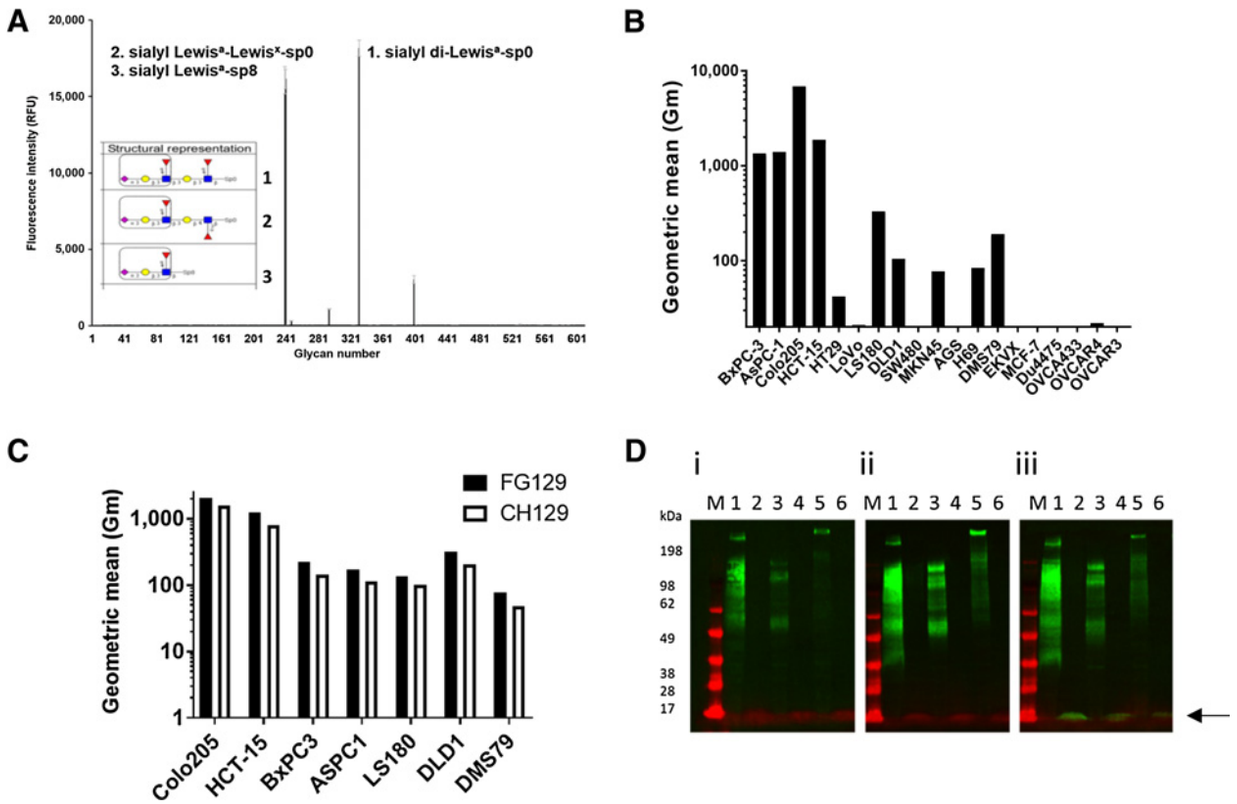

Figure 1.

Sialylated glyco-epitope recognition on cancer cell surface glycoproteins by FG129 and CH129. **A,** Fine binding specificity of FG129 by high-density glycan array screening (CFG, core H, version 5.1). 'Sp' denotes the length of the spacer between the glycan and the slide. Inset shows the top binding glycan structures as listed in Supplementary Table S2. The complete results for FG129 have been deposited on the CFG website. **B,** Overview of FG129 binding (33.3 nmol/L) to a range of pancreatic, colorectal, gastric, lung, and breast cancer cell lines via indirect immunofluorescence staining and flow cytometric analysis. **C,** Comparison of cell surface binding by CH129 of a subset of cancer cell lines compared with FG129 (33.3 nmol/L) via indirect immunofluorescence staining and flow cytometric analysis. **D,** Western analysis of cell lysates and total lipid (TL) extract from selected colorectal and pancreatic cancer cell lines. i, FG129; ii, CH129; iii, CA19.9 mAb (SPM110). Lane M, molecular marker; lane 1, COLO205 cell lysates (1 $\times$ 10^5 cells); lane 2, COLO205 TL (1 $\times$ 10^6 cells); lane 3, HCT-15 cell lysates (1 $\times$ 10^5 cells); lane 4, HCT-15 TL (1 $\times$ 10^6 cells); lane 5, BxPC3 cell lysates (1 $\times$ 10^5 cells); lane 6, BxPC3 TL (1 $\times$ 10^6 cells). The 129 mAbs only bound glycoprotein species, in contrast to the CA19.9 mAb SPM110 that also recognizes sialyl-Lewis^a on glycolipids, which do not resolve on SDS-PAGE and run at the dye front (arrow).

Published OnlineFirst December 23, 2019; DOI: 10.1158/1535-7163.MCT-19-0221

Table 1. Determination of FG129 and CH129 functional affinity for sialyl-Lewis[a]-APD-HSA and cancer cell surface.

	SPR Real-time sialyl-Lewis[a]-APD-HSA binding[a,b]			FACS Cell surface binding	ELISA Sialyl-Lewis[a]-APD-HSA binding
mAb	Association rate, k_{on} (1/Ms)	Dissociation rate, k_{off} (1/s)	Dissociation constant, K_d (nmol/L)	Dissociation constant, K_d (nmol/L)	Half maximal effective concentration, EC_{50} (nmol/L)
FG129	6.2×10^5	1.1×10^{-4}	0.18	21	0.3
CH129	4.5×10^5	8.2×10^{-5}	0.18	59	0.6

[a]High-density SPR chip.
[b]The apparent binding affinity for FG129 and CH129 on the low-density chip was 43 nmol/L and 21 nmol/L, respectively.

ASPC1. Crucially, FG129 did not bind granulocytes or lymphocytes from a representative normal blood donor (Supplementary Fig. S1B) nor did FG129 bind to normal HUVECs (Supplementary Fig. S1C). These results identified several high-binding colorectal as well as pancreatic cancer cell lines with which to assess FG129-based therapeutic modalities *in vitro*.

A clinically more relevant hIgG1 chimeric variant, CH129, was created via cloning of the FG129 heavy- and light-chain variable sequences in-frame with the hIgG1 constant regions. CH129 bound a similar range of cancer cell lines compared with FG129 (**Fig. 1C**), with strong binding observed on COLO205 and HCT-15, moderate binding to DLD1, BxPC3, ASPC1, and LS180 and low binding on DMS79.

On the cancer cell surface, glyco-epitopes can be present on glycoproteins as well as glycolipids. Consequently, we assessed recognition of biologically relevant glyco-targets by FG129 and CH129, in more detail, by Western blotting using total lipid cell extracts and whole-cell lysates from colorectal (COLO205 and HCT-15) and pancreatic (BxPC3) cell lines. FG129, as well as CH129, bound to a range of predominantly high-molecular weight (50–200 kDa) glycoproteins in all lysates, with more intense staining observed for COLO205 compared with the HCT-15 and BxPC3 lysates, potentially reflecting the differences in ABC (**Fig. 1D**). Interestingly, both the COLO205 and BxPC3 staining patterns displayed a band of very high molecular weight, not observed for the HCT-15 lysate, perhaps suggesting mucin binding. In comparison, the CA19.9 glycan as defined by mAbs 19-9 and 52a is a monosialoganglioside, a sialylated glycolipid derivative of lacto-*N*-fucopentaose II (20, 34). Accordingly, Western blot analysis of the same cell lysates and total lipid extracts with CA19.9-recognizing SPM110 showed a prominent glycolipid band at the dye front, in all three total lipid extracts, as well as a number of glycoprotein species (**Fig. 1D**).

FG129 and CH129 bind their glycotarget with nanomolar functional affinity, *in vitro* and on the cell surface

The glycome analysis indicated that the preferred glyco-target of FG129 was sialyl-di-Lewis[a] closely followed by sialyl-Lewis[a], but only if presented on a complex sugar or long carbon spacer. As sialyl-di-Lewis[a] was not commercially available as a conjugate, we opted for a sialyl Lewis [a]–HSA conjugate with the glycan linked to HSA lysine residues via an extended acetyl phenylene diamine (APD) spacer, for performing *in vitro* binding studies. We thus set out to measure FG129 and CH129 functional affinity using the aforementioned glycan conjugate and SPR analysis, as well as through ELISA. SPR affinity measurements of FG129 and CH129 on the sialyl-Lewis[a]-APD-HSA–coupled CM5 chip revealed functional affinity of the order of 0.1 nmol/L on the high-density surface, governed by fast on-rates (10^5 Ms^{-1}) and a slow off-rates (10^{-4} s^{-1}; **Table 1**) and monovalent nanomolar (~10 nmol/L) affinity, on the low-density surface. In addition, concentration-dependent sialyl-Lewis[a]-APD-HSA antigen binding was assessed by ELISA, where FG129 as well as CH129 bound sialyl-Lewis[a]-APD-HSA with subnanomolar EC_{50} (**Table 1**; Supplementary Fig. S2A). Cancer cell surface functional affinity was assessed using flow cytometry and fitting the results to a one-site specific binding model, after subtraction of nonspecific binding. This revealed an apparent nanomolar K_d for FG129 and CH129 on COLO205 (Supplementary Fig. S2B; **Table 1**) as well as HCT-15 and BxPC3 (Supplementary Fig. S2C and S2D, respectively).

FG129's glyco-epitope distribution covers an extended range of human tumor tissues, combined with minimal normal tissue cross-reactivity

The tumor tissue binding of FG129 was assessed by IHC. FG129 bound to 74% (135/182) of pancreatic tumors, 50% (46/92) of gastric tumors, 36% (100/281) of colorectal tumors, 27% (89/327) of ovarian, and 21% (42/201) of NSCLC tumors (**Table 2**). Representative images of different staining levels of tumor tissues are shown in **Fig. 2A**. In the pancreatic cancer cohort, Kaplan–Meier analysis of disease-free survival of patients with pancreatic revealed a significantly lower mean survival time in the high FG129–binding group (high, mean survival: 30 months ($n = 94$)) compared with the lower FG129 binding group (low, mean survival: 90 months; $n = 82$; $P = 0.004$, log-rank test). On multivariate analysis using Cox regression, high FG129 antigen expression in pancreatic cancer was a marker for poor prognosis which was independent of perineural invasion and lymph node involvement ($P = 0.012$) which are key prognostic factors in pancreatic cancer. This suggests that in this cohort, patients with high-density glyco-epitope expression would benefit from FG129-based therapy.

The normal tissue distribution of FG129 was evaluated using two normal human TMAs: AMSbio, T8234708-5, covering 31 tissues, one normal human individual per tissue, in duplicate, and US Biomax, FDA999i, 32 types of normal organs from three individuals, single core per case. On the AMSbio array, FG129 displayed a very restricted binding pattern and did not bind most normal tissues, including vital tissues such as heart, brain, stomach, and kidney (Supplementary Table S3; **Fig. 2C**). Weak to moderate binding of a very small percentage of cells was seen in gallbladder, ileum, liver, esophagus, pancreas, and thyroid. In contrast, the CA19.9 mAb stained a subset of tissues: esophagus, liver, and pancreas with strong intensity (Supplementary Table S3). In addition, the majority of tissues on the US Biomax array were negative with low-to-moderate staining of a small fraction of cells on tonsils (1/3), thymus (2/3); salivary gland (1/3); esophagus (3/3); adjacent normal (1/3), and cancer adjacent uterine cervix tissue (2/3; Supplementary Fig. S3).

Published OnlineFirst December 23, 2019; DOI: 10.1158/1535-7163.MCT-19-0221

Table 2. Binding of FG129 (7.4 nmol/L) by IHC to gastric, colorectal, pancreatic, ovarian, and lung TMAs, by staining intensity.

Tissue	Gastric	Colorectal	Pancreatic/biliary/ampullary	Ovarian	Lung (adenocarcinoma)
			Staining (%) (*n*/total)		
Negative	50 (46/92)	64 (181/281)	25 (45/180)	73 (238/327)	79 (159/201)
Weak	27 (25/92)	26 (72/281)	21 (37/180)	19 (63/327)	10 (21/201)
Moderate	11 (10/92)	9 (25/281)	34 (61/180)	6 (21/327)	4 (9/201)
Strong	12 (11/92)	1 (3/281)	21 (37/180)	2 (5/327)	6 (12/201)

FG129 recognizes secreted glyco-antigen in the serum of patients with pancreatic cancer and a mouse COLO205 xenograft model, but not healthy donors

CA19.9 can be expressed on glycolipid (monosialoganglioside) as well as mucins and detection of this antigen in sera of pancreatic and colorectal cancer is used in clinical practice to monitor disease progression and response to therapy (16, 23, 35). This is currently the only FDA-approved test for pancreatic cancer. As FG129 detects terminal/accessible sialyl-Lewis^a–containing glycoproteins, we analyzed a subset of patient sera from our pancreatic cancer cohort for the presence of glyco-antigen using sandwich ELISA. No secreted glyco-antigen was detected in 12 sera from healthy donors, whereas in 33% (7/21) pancreatic cancer sera, glyco-antigen levels were significantly raised (**Fig. 3A**). Similarly, serum from a mouse COLO205 xenograft model, included as a positive control, also contained significantly elevated secreted glyco-antigen (**Fig. 3A**). We next set out to investigate whether the presence of secreted glyco-antigen would impede tumor cell binding, using flow cytometry. FG129 was preincubated at 37ºC with the relevant sera, after which cell binding to HCT-15 was evaluated (**Fig. 3B**). FG129 maintained HCT-15 binding after preincubation with patients' sera, suggesting that its nanomolar cell surface functional affinity is sufficient to retain tumor cell targeting, even in the presence of secreted glyco-antigen.

Efficient cellular internalization of FG129 as well as CH129 and delivery of indirectly conjugated payload on high-binding cancer cells

As the murine and human 129 mAbs displayed avid glycotarget binding on high-binding colorectal and pancreatic cancer cell lines, we sought to analyze their internalization potential. Confocal microscopy of Alexa Fluor 488–labeled FG129 and CH129, incubated with COLO205 cells for 60 to 90 minutes, showed very efficient internalization of both mAbs with a significant proportion colocalizing with lysosomal compartments, as well as a proportion remaining on the cell surface (**Fig. 4A**). Similar results were obtained using HCT-15 and BxPC3 (Supplementary Fig. S4A and S4B, respectively), suggesting that high-level 129 mAb binding at the cell surface drives target internalization.

Lysosomal targeting by the 129 mAbs was further validated through assessing the toxicity of saporin ("ZAP", IT-48, ATS Bio)-conjugated anti-mouse/human Fab immune complexes containing FG129 or CH129 on high-binding cancer cell lines. Internalization of Fab-ZAP-FG129 led to a dose-dependent decrease in cell viability (EC_{50} ~ 1 pmol/L) on high-binding cells COLO205 and HCT-15 but surprisingly, not on BxPC3 (**Fig. 4B**, i). *MUC1* expression by BxPC3 has been linked to chemoresistance as a result of increased expression of multidrug resistance (MDR) genes (36). The antigen-low cell line LoVo was refractory to Fab-ZAP-FG129 with a modest inhibition of viability only at the highest concentrations. Fab-ZAP preincubated with isotype control showed negligible cytotoxicity. Importantly, this was corroborated for CH129, where the saporin-conjugated CH129 displayed dose-dependent toxicity with picomolar EC_{50} on the high-binding COLO205 and HCT-15 (**Fig. 4B**, ii). Together, the results indicate efficient internalization and payload delivery in high-binding cancer cell lines by FG129 and CH129. Advantageously, in addition to their efficient internalization, the 129 mAbs retained potent ADCC effector activity on the high-binding COLO205 (**Fig. 4C**), and HCT-15 (Supplementary Fig. S4C), with EC_{50} values in the subnanomolar range (~0.1 nmol/L), indicating that the glyco-proteins associated with mAb internalization are distinct from the ones targeted for effector functions and suggests multimodal development potential.

CH129–drug conjugate (ADC) shows high *in vitro* activity on high-binding cancer cell lines

To directly assess the ADC potential of CH129, we conjugated it to clinically validated linker/payload combinations (**Fig. 5A**), as described in the Materials and Methods Section (DAR; Supplementary Table S1) and compared their cytotoxicity to that of a nontargeting RTX-ADC control on the high-binding colorectal cancer cell lines COLO205 and HCT-15. *In vitro* cytotoxicity analysis of the CH129–ADC constructs on high-binding COLO205 showed potent toxicity of all three CH129–ADC constructs, CH129-vcE (65.8 pmol/L EC_{50}), CH129-SMCC-DM1 (0.2 nmol/L EC_{50}) and CH129-SPDP-DM4 (0.1 nmol/L EC_{50}), and 100% inhibition at the highest concentration tested (**Fig. 5B**; Supplementary Table S4). Activity of the CH129-ADC compounds on HCT-15 (**Fig. 5C**) was lower compared with COLO205, with nanomolar EC_{50} values for all three CH129-ADC constructs (Supplementary Table S4). HCT-15 was more resistant to killing by the CH129–ADC constructs, cell survival being about 30%–40% at the highest concentration tested, possibly due to the presence of MDR1 or other ATP-dependent efflux systems (37). On the pancreatic line BxPC3, EC_{50} values were in the low nanomolar range (**Fig. 5D**; Supplementary Table S4). On COLO205 and BxPC3, CH129-vcE, with the peptidase-cleavable linker, outperformed the noncleavable linker-containing ADCs. The nontargeting control RTX-vcE showed no cytotoxicity over the entire concentration range tested, whereas RTX-DM1 only showed significant activity at the highest concentration (100 nmol/L). RTX-DM4 displayed more potent nonspecific toxicity (Supplementary Table S4), potentially due to its slightly higher DAR compared with the other control ADCs (Supplementary Table S1).

Cytotoxicity assays on cell mixtures containing increasing amounts of glyco-antigen–negative cells (AGS) in combination with the high-binding COLO205 were performed to assess the potential for bystander killing by CH129–ADC conjugates with cleavable linkers, such as the CH129-vcE and CH129-SPDP-DM4, and thus the possibility of targeting heterogeneous tumors containing cells expressing lower amounts or no glyco-target, as well as tumor stromal cells. The two

Published OnlineFirst December 23, 2019; DOI: 10.1158/1535-7163.MCT-19-0221

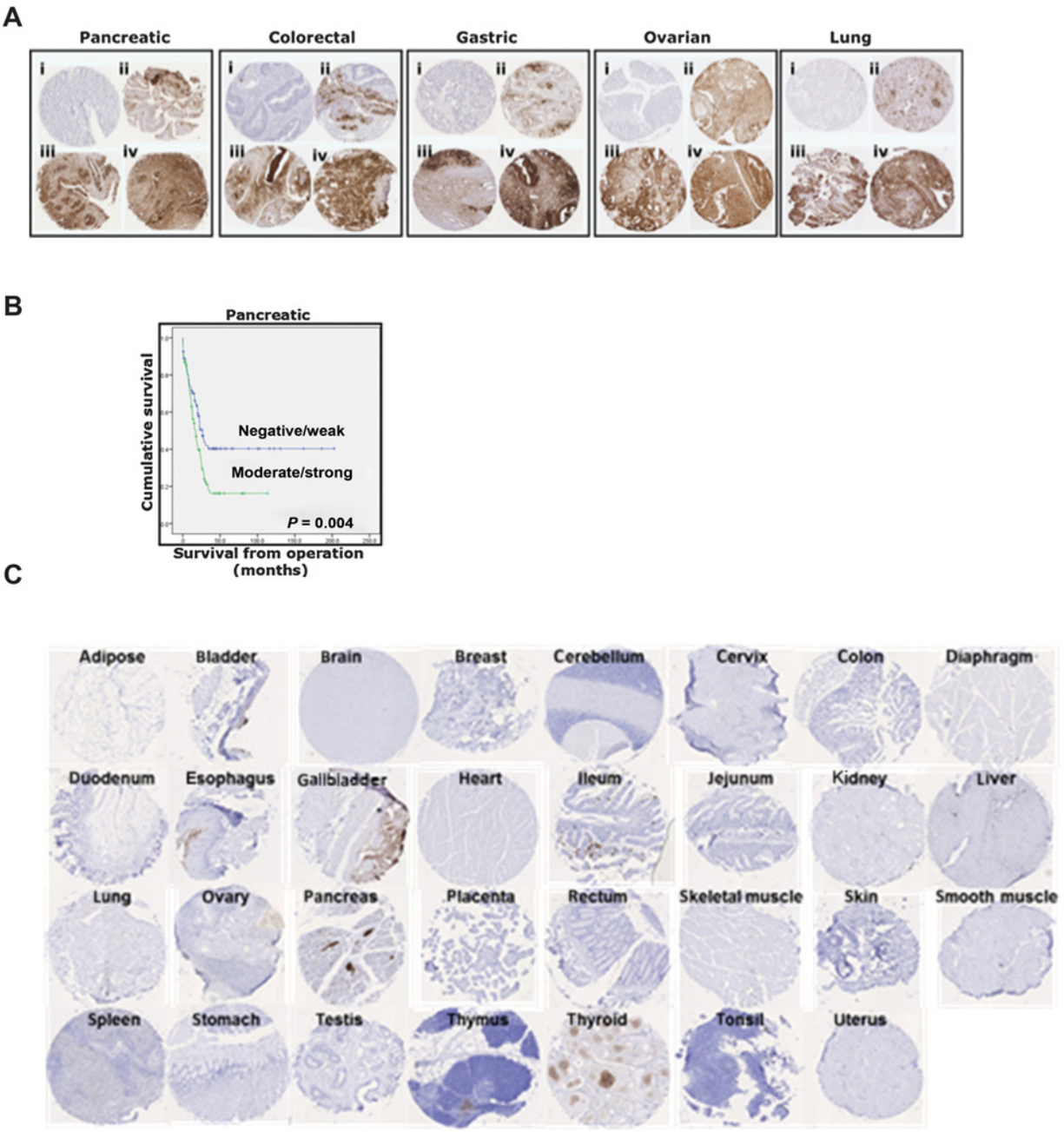

Figure 2.

Strong differential tumor versus normal human tissue distribution via IHC of the FG129. **A,** Binding of FG129 (7.4 nmol/L) by IHC to pancreatic, colorectal, gastric, ovarian, and lung TMAs. Representative images of different staining levels are shown: (i) negative, (ii) weak, (iii) moderate, and (iv) strong (magnification ×20). **B,** Kaplan–Meier analysis of disease-free survival in the pancreatic patients' cohort after TMA staining with FG129. Cutoff for high versus low was determined by X-tile. **C,** Normal human tissue (AMSBIO) binding of FG129, showing limited binding in esophagus, gallbladder, ileum, liver, pancreas, and thyroid (magnification ×20).

CH129-ADC constructs with cleavable linkers and thus bystander potential comprised CH129-vcE and CH129-SPDP-DM4, whereas CH129-SMCC-DM1, with its uncleavable linker, was used as a control in these experiments. A fixed amount of antigen-positive COLO2025 cells was mixed with increasing amounts of antigen-negative AGS cells and cell killing by the CH129-ADC compounds analyzed at 1 nmol/L. This concentration was chosen for maximum killing of COLO205 and at the same time absence of killing of antigen-negative AGS cells (Supplementary Fig. S5). Only CH129-DM4 maintained its COLO205 killing activity in the presence of increasing amounts of antigen-negative AGS cells, inducing over 50% killing at a ratio of 10:1 of AGS:COLO205 cells; CH129-vcE displayed intermediate bystander killing, showing a gradual decrease in killing activity with increasing amounts of AGS cells (**Fig. 5E**). Finally, CH129-DM1 with its

Published OnlineFirst December 23, 2019; DOI: 10.1158/1535-7163.MCT-19-0221

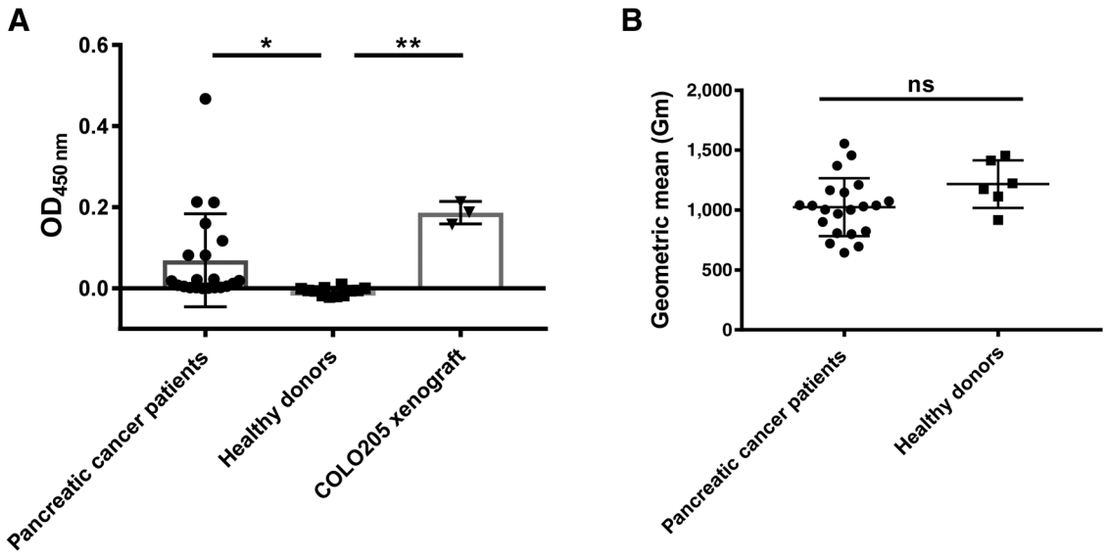

Figure 3.

A, Sandwich ELISA using FG129 for the detection of secreted sialyl-di-Lewis^a in sera from patients with pancreatic cancer ($n = 21$), healthy human donors ($n = 12$), as well as a mouse COLO205 xenograft model ($n = 3$). Significance was deduced from one-way ANOVA with Bonferroni corrections for multiple comparisons. **B,** Competition flow cytometry–based assay showing AlexaFluor 488–labeled FG129 binding to HCT-15 cells, following preincubation with sera from patients with pancreatic cancer compared with sera from five healthy human donors. FG129 maintains cell surface binding in the presence of secreted glyco-antigen (ns, unpaired *t* test). *< 0.05; **< 0.01; ns, not significant.

uncleavable linker required a near homogenous COLO205 population to induce cell killing. Combined, the results suggest linker cleavability dependent bystander killing by CH129-DM4 as well as CH129-vcE.

CH129–vcE conjugate potently controls tumor growth *in vivo* in a COLO205 xenograft model

On the basis of the subnamolar *in vitro* killing potency (65.8 pmol/L EC_{50}) as well as its intermediate bystander killing activity, we selected CH129-vCE for evaluation of *in vivo* tumor control in a COLO205 xenograft model. Tumors were established and dosing started on day 7. In this model, biweekly administration of four doses of CH129-vcE established a significant reduction in tumor volume compared with the control ADC, RTX-vcE (two-way ANOVA, $P < 0.0001$; **Fig. 6A**). Impressively, 7 of 10 mice became tumor-free for the duration of the study. The compounds were well-tolerated, with no adverse effects on mean body weight (**Fig. 6B**).

Discussion

We have generated a mouse IgG1k anti-sialyl-di-Lewis^a (Neu5Acα2-3Galβ1-3(Fucα1-4)GlcNAcβ1-3Galβ1-3(Fucα1-4)-GlcNAcβ) mAb, as well as a chimeric hIgG1 variant. The mAb only bound mono-sialyl-Lewis^a if presented on a long carbon spacer suggesting a preference for accessible (terminal) sialyl-Lewis^a -containing glycan. Importantly, no cross-reactivity with the dietary-derived Neu5Gc-Lewis^a was observed. Characterization of the cell surface glycotarget of our 129 mAb suggests it to be selectively expressed on glycoproteins; predominantly, but not exclusively, on colorectal, pancreatic, and gastric cancer cell lines. In contrast, the CA19.9 targeting mAb, SPM110, bound both glycolipids and glycoproteins upon Western analysis. This differential binding profile may be the result of differing binding affinities, combined with the distinctive glycan clustering patterns of glycoproteins compared with lipid-associated glycans. In addition, the fine-binding specificities of the two mAbs may contribute to their differing target binding profile. In this context, SPM110 has been shown to cross-react with Neu5Gc-Lewis^a (CFG, primscreen_5461). In addition, a recent comparison of a selection of CA19-9 targeting mAbs, currently used in clinical diagnostics, demonstrated varied recognition of Neu5Ac- as well as Neu5Gc-conjugated glycans (38).

Both 129 mAbs (FG129 (mIgG1) as well as CH129 (chimeric hIgG1) displayed high functional sialyl Lewis^a binding affinity: K_d ~0.2 nmol/L and 20–50 nmol/L on high- and low-density surfaces (SPR), respectively, likely reflecting the target density-dependent differential binding modes (bivalent versus monovalent). ELISA experiments yielded similar EC_{50} values compared with SPR, whereas cell surface binding functional affinity was slightly reduced, albeit still in the nanomolar range, presumably due to the more fluid nature of the cell membrane and the occurrence of other biological processes such as internalization (27). The findings may also reflect the different target antigen utilized (sialyl-Lewis^a-APD-HSA in ELISA and SPR vs. complex glycoproteins on the cell surface). Taken together the apparent nanomolar functional affinity should enable robust tumor targeting (39).

The 129 mAb glyco-target displayed a wide tumor tissue distribution encompassing pancreatic, colorectal, and gastric cancers, as well as ovarian and NSCLC to a lesser degree. Increased sialylation is associated with enhanced proliferative and metastatic potential of both colorectal and pancreatic cancer, rendering sialyl-di-Lewis^a targeting therapy an attractive option (22, 40–42). Earlier work has demonstrated the prognostic value of serum secreted sialyl-Lewis^a in pancreatic adenocarcinoma (23, 43). Our study reveals that the FG129 glyco-epitope expression in pancreatic cancer is also an independent marker for poor prognosis, suggesting that therapy based on the 129 mAb would have the highest impact on the more aggressive tumors. In addition, we found that FG129 recognized secreted sialyl-di-Lewis^a in around 30% of the pancreatic patients' sera, whereas

Published OnlineFirst December 23, 2019; DOI: 10.1158/1535-7163.MCT-19-0221

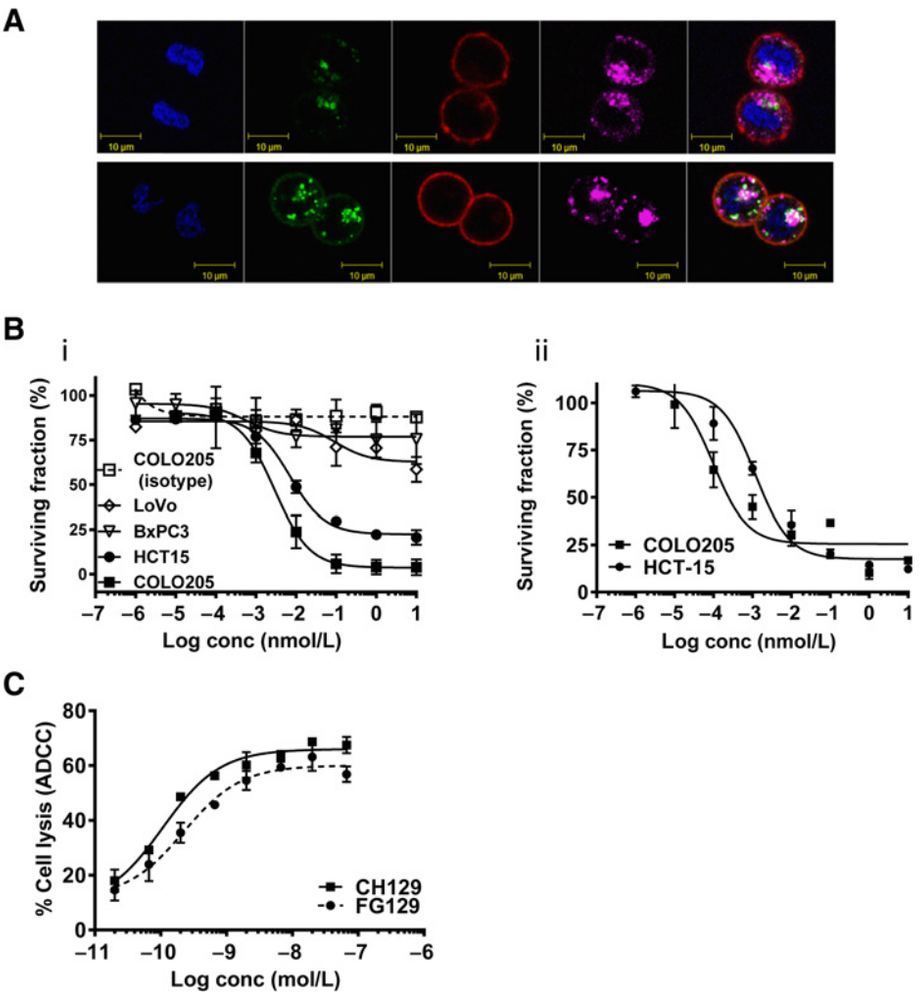

Figure 4.

A, Effective cellular internalization and lysosomal targeting do not affect immune effector functions by FG129 and CH129. Z-stack confocal microscopy of Alexa Fluor 488–labeled FG129 (top) and CH129 (bottom) internalization in COLO205 cells, showing colocalization with lysosomal compartments. The plasma membrane was labeled with CellMask Orange (red), the lysosomes with LysoTracker Deep Red (purple), and the nucleus with Hoechst 33258 (blue; magnification ×60). **B,** Lysosomal saporin delivery by FG129 (i) and CH129 (ii). Cytotoxicity of Fab-ZAP-FG129 on COLO205, HCT-15, BxPC3, and LoVo cells was evaluated using 3H-thymidine incorporation as described in Materials and Methods (i). Cytotoxicity of Fab-ZAP-CH129 on COLO205 and HCT-15 cells (ii). In both cases, normalized results are presented as a percentage of the proliferation of cells treated with the primary mAb only. Error bars, mean ± SD from four independent experiments. **C,** ADCC activity with subnanomolar potency of CH129 and FG129 on COLO205.

negligible secreted target was detected in the serum from healthy individuals. This is a reduced frequency compared with the current diagnostic/prognostic CA19.9–based detection levels that frequently detect secreted antigen in 62%–68% of pancreatic cancer patients' sera (38) and may reflect the different binding specificities as well as affinities of the mAbs. Critically, under conditions mimicking *in vivo* application, the FG129 maintained binding to its cell surface glyco-target in the presence of secreted antigen, suggesting that secreted circulating glyco-antigen may not be detrimental to 129 mAb tumor targeting. Normal human tissues displayed very restricted 129 glyco-epitope expression. Vital tissues such as heart, brain, lungs, and kidneys were all negative, as well as most other nonvital tissues. Weak to moderate FG129 binding was observed to normal gallbladder, ileum, liver, esophagus, pancreas, and thyroid, but only on a small fraction of cells. This differential tissue binding profile with strong tumor tissue reactivity and limited normal tissue cross-reactivity, renders the 129 mAb an attractive candidate for clinical development.

FG129 exhibited very efficient cellular internalization and lysosomal localization as demonstrated by two indirect approaches, confocal microscopy and targeted toxin delivery. Internalization of indirectly toxin-conjugated 129 mAbs led to killing of high-binding colorectal cancer cell lines with picomolar EC_{50}. The internalization was directly dependent on the cell surface antigen density in cell lines, with high glyco-epitope–expressing cell lines internalizing better than low-density–expressing cell lines. On that basis, we directly conjugated CH129 with three clinically validated linkers and drugs [auristatin (vcMMAE, cleavable) as wells as maytansinoids (SMCC-DM1, uncleavable and SPDP-DM4, moderately cleavable] thereby covering a range of linker chemistries, as well as bystander killing potential. All three CH129-ADCs exhibited subnanomolar killing of high-binding colorectal cancer lines and nanomolar killing on moderately binding colorectal cancer as well as pancreatic cell lines. CH129-vcMMAE consistently exhibited the most potent killing against uniform cells, whereas CH129-DM4 exerted the most efficient bystander killing in mixed (antigen-positive and negative cells) cultures. As such, CH129-vcMMAE exerted potent *in vivo* tumor control in a COLO205 xenograft model. Interestingly, our analysis indicated that the sera from mice with established tumors contained secreted glyco-antigen; however, this did not impeded the significant *in vivo* activity of CH129-vcE. Alternative site-specific conjugation strategies, as well as more potent drugs, for example the very potent Pyrrolobenzodiazepine (PBD), that are currently being evaluated, would constitute attractive alternatives for conjugation to the 129 mAb (44, 45).

Importantly, in addition to drug conjugate potential, the 129 mAb maintains strong ADCC effector function, suggesting that alternative approaches with cancer targeting utility could be adopted. These include T-cell redirecting bispecific (TCB) formats in combination with an anti-CD3 arm, as well as the use of the 129 variable regions for reformatting for chimeric antigen receptor (CAR)-T approaches, both

Published OnlineFirst December 23, 2019; DOI: 10.1158/1535-7163.MCT-19-0221

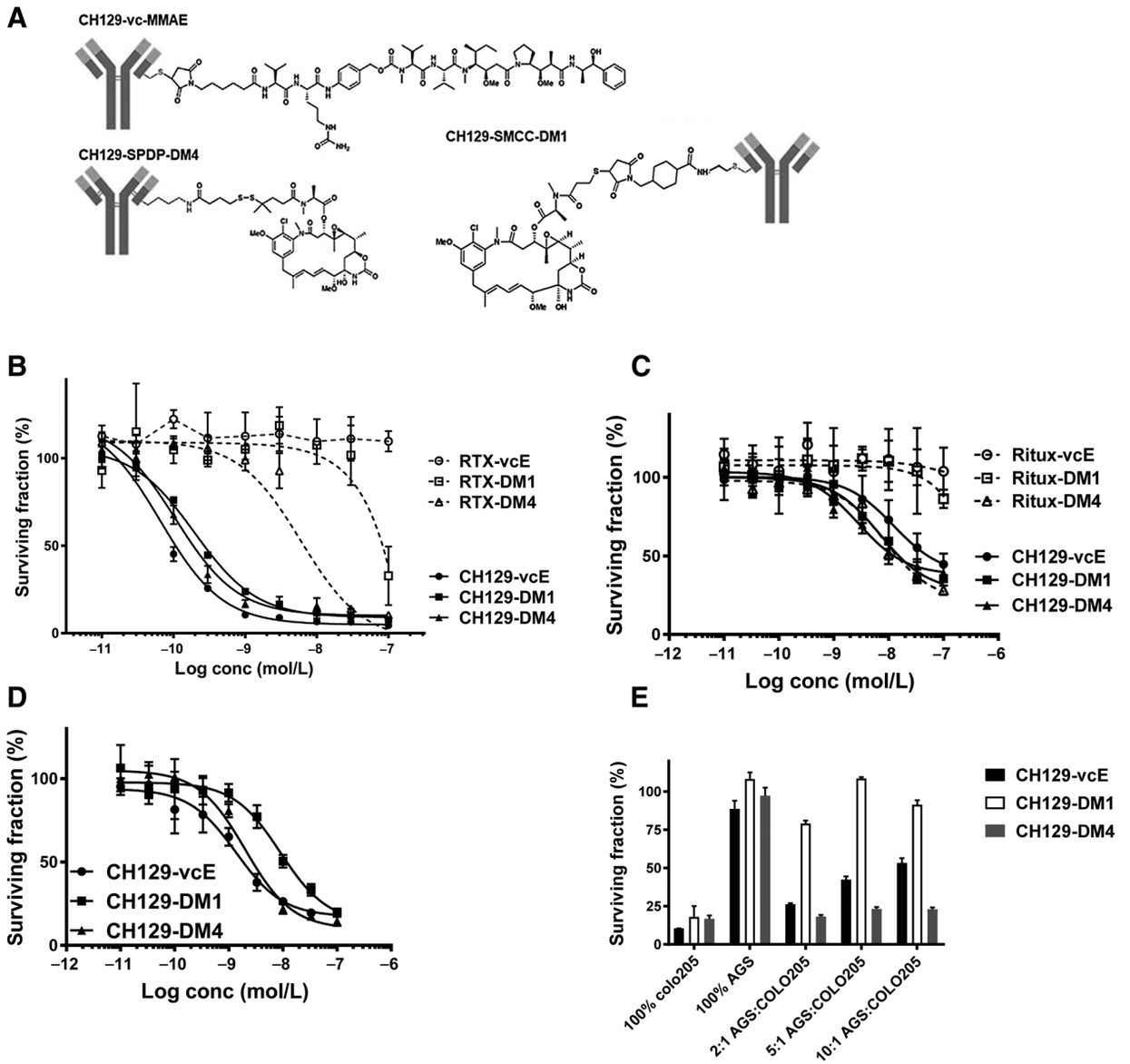

Figure 5.

A, Potent *in vitro* cytotoxicity of CH129–ADC compounds on colorectal and pancreatic cell lines. Schematic drawing of the three CH129-ADC compounds used in this study. *In vitro* cytotoxicity of activity of CH129-ADC compounds on COLO205 (**B**); HCT-15 (**C**), and BxPC3 (**D**). **E,** Bystander killing activity of CH129-ADC compounds at 1 nmol/L in mixed cultures of antigen-positive (COLO205) and antigen-negative (AGS) cells.

of which rely on minimal normal tissue cross-reactivity (46). Recently, an attractive strategy for increased tumor-specific targeting in the TCB setting was proposed in the shape of an avidity-optimized HER2 TCB (47). This strategy hinged on the combination of low monovalent target affinity, precluding normal tissue (with low target expression) binding, with avidity-driven tumor targeting and this approach could be relevant for the 129 mAb.

In this global immuno-oncology era, cancer-associated sialylated glycans constitute attractive targets for cancer immunotherapy. The immunologic consequences of aberrant cancer cell surface expression of sialic acid–containing glycoconjugates range from disabling the killing mechanisms of effector cells, increasing the production of immunosuppressive cytokines, complement regulation, as well as reducing the activation of antigen-presenting cells, many aspects of which are governed by the interaction with immune-inhibitory siglec receptors (9, 10, 13, 48–50). This was recently substantiated by data demonstrating that sialic acid blockade had a major impact on tumor immune cell composition and effector cell killing ability, creating an immune-permissive tumor microenvironment (51).

In conclusion, our sialyl-di-Lewis^a-targeting 129 mAb with restricted normal tissue binding combined with a wide-ranging tumor distribution, favorable functional target affinity, as well as efficient internalization and potential multimodal application, constitutes an attractive candidate for cancer immunotherapy.

Published OnlineFirst December 23, 2019; DOI: 10.1158/1535-7163.MCT-19-0221

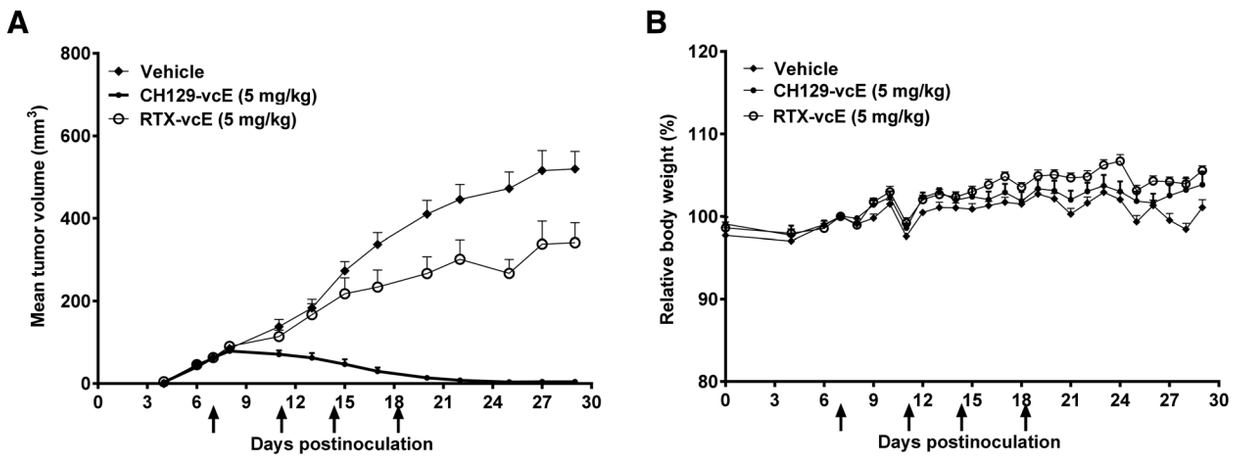

Figure 6.

Potent i*n vivo* tumor control by CH129-vcE ADC in a COLO205 xenograft model. **A**, Significant ($P < 0.0001$) *in vivo* tumor control by 129-vcE compared with vehicle control and compared with the nontargeting RTX-vcE in a COLO205 xenograft model (Balb/c mice). **B,** No significant adverse effect was observed on mean body weight during the course of the study. Arrows indicate day of dosing. Significance was deduced from two-way ANOVA with Bonferroni corrections for multiple comparisons.

Disclosure of Potential Conflicts of Interest

S.T. Tivadar reports receiving a commercial research grant from Scancell Ltd (during PhD studies, received a scholarship from Scancell Ltd covering 2 years of tuition fees and stipend). L.G. Durrant is a CSO, reports receiving a commercial research grant from, and has ownership interest (including patents) in Scancell Ltd. No potential conflicts of interest were disclosed by the other authors.

Authors' Contributions

Conception and design: S.T. Tivadar, T. Parsons, L.G. Durrant, M. Vankemmelbeke
Development of methodology: S.T. Tivadar, R.S. McIntosh, A.M. Zaitoun, M. Vankemmelbeke
Acquisition of data (provided animals, acquired and managed patients, provided facilities, etc.): S.T. Tivadar, R.S. McIntosh, A.M. Zaitoun, S. Madhusudan
Analysis and interpretation of data (e.g., statistical analysis, biostatistics, computational analysis): S.T. Tivadar, R.S. McIntosh, A.M. Zaitoun, L.G. Durrant, M. Vankemmelbeke
Writing, review, and/or revision of the manuscript: T. Parsons, A.M. Zaitoun, S. Madhusudan, L.G. Durrant, M. Vankemmelbeke
Administrative, technical, or material support (i.e., reporting or organizing data, constructing databases): S.T. Tivadar, R.S. McIntosh, J.X. Chua, R. Moss, S. Madhusudan
Study supervision: L.G. Durrant
Other (assessed in pathology): A.M. Zaitoun

Acknowledgments

We are grateful for confocal imaging assistance by Tim Self (School of Life Sciences, University of Nottingham, Nottingham, United Kingdom), as well as for Biacore access (Prof. Stephanie Allen, School of Pharmacy, University of Nottingham, Nottingham, United Kingdom). This work was supported by grants from the MRC (RA4850; to L.G. Durrant).

The costs of publication of this article were defrayed in part by the payment of page charges. This article must therefore be hereby marked *advertisement* in accordance with 18 U.S.C. Section 1734 solely to indicate this fact.

Received March 4, 2019; revised October 25, 2019; accepted December 9, 2019; published first December 23, 2019.

References

1. Drake RR. Glycosylation and cancer: moving glycomics to the forefront. Adv Cancer Res 2015;126:1–10.
2. Daniotti JL, Vilcaes AA, Torres Demichelis V, Ruggiero FM, Rodriguez-Walker M. Glycosylation of glycolipids in cancer: basis for development of novel therapeutic approaches. Front Oncol 2013;3:306.
3. Dalziel M, Crispin M, Scanlan CN, Zitzmann N, Dwek RA. Emerging principles for the therapeutic exploitation of glycosylation. Science 2014;343:1235681.
4. Pinho SS, Reis CA. Glycosylation in cancer: mechanisms and clinical implications. Nat Rev Cancer 2015;15:540–55.
5. Varki A, Kannagi R, Toole BP. Glycosylation changes in cancer. In: Varki A, Cummings RD, Esko JD, Freeze HH, Stanley P, Bertozzi CR, et al., editors. Essentials of glycobiology. New York, NY: Cold Spring Harbor; 2009.
6. Rodrigues JG, Balmana M, Macedo JA, Pocas J, Fernandes A, de-Freitas-Junior JCM, et al. Glycosylation in cancer: selected roles in tumor progression, immune modulation and metastasis. Cell Immunol 2018;333:46–57.
7. Cagnoni AJ, Perez Saez JM, Rabinovich GA, Marino KV. Turning-off signaling by siglecs, selectins, and galectins: chemical inhibition of glycan-dependent interactions in cancer. Front Oncol 2016;6:109.
8. Beatson R, Tajadura-Ortega V, Achkova D, Picco G, Tsourouktsoglou TD, Klausing S, et al. The mucin MUC1 modulates the tumor immunological microenvironment through engagement of the lectin Siglec-9. Nat Immunol 2016;17:1273–81.
9. Stanczak MA, Siddiqui SS, Trefny MP, Thommen DS, Boligan KF, von Gunten S, et al. Self-associated molecular patterns mediate cancer immune evasion by engaging Siglecs on T cells. J Clin Invest 2018;128:4912–23.
10. Hudak JE, Canham SM, Bertozzi CR. Glycocalyx engineering reveals a Siglec-based mechanism for NK cell immunoevasion. Nat Chem Biol 2014;10:69–75.
11. Macauley MS, Paulson JC. Immunology: glyco-engineering 'super-self'. Nat Chem Biol 2014;10:7–8.
12. Sweeney JG, Liang J, Antonopoulos A, Giovannone N, Kang S, Mondala TS, et al. Loss of GCNT2/I-branched glycans enhances melanoma growth and survival. Nat Commun 2018;9:3368.
13. Bull C, Stoel MA, den Brok MH, Adema GJ. Sialic acids sweeten a tumor's life. Cancer Res 2014;74:3199–204.
14. Dall'Olio F, Malagolini N, Trinchera M, Chiricolo M. Sialosignaling: sialyltransferases as engines of self-fueling loops in cancer progression. Biochim Biophys Acta 2014;1840:2752–64.
15. Sato M, Narita T, Kimura N, Zenita K, Hashimoto T, Manabe T, et al. The association of sialyl Lewis(a) antigen with the metastatic potential of human colon cancer cells. Anticancer Res 1997;17:3505–11.

16. Matsui T, Kojima H, Suzuki H, Hamajima H, Nakazato H, Ito K, et al. Sialyl Lewisa expression as a predictor of the prognosis of colon carcinoma patients in a prospective randomized clinical trial. Jpn J Clin Oncol 2004;34:588–93.
17. Kishimoto T, Ishikura H, Kimura C, Takahashi T, Kato H, Yoshiki T. Phenotypes correlating to metastatic properties of pancreas adenocarcinoma in vivo: the importance of surface sialyl Lewis(a) antigen. Int J Cancer 1996;69:290–4.
18. Perdicchio M, Cornelissen LA, Streng-Ouwehand I, Engels S, Verstege MI, Boon L, et al. Tumor sialylation impedes T cell mediated anti-tumor responses while promoting tumor associated-regulatory T cells. Oncotarget 2016;7:8771–82.
19. Magnani JL, Nilsson B, Brockhaus M, Zopf D, Steplewski Z, Koprowski H, et al. A monoclonal antibody-defined antigen associated with gastrointestinal cancer is a ganglioside containing sialylated lacto-N-fucopentaose II. J Biol Chem 1982;257: 14365–9.
20. Magnani JL, Brockhaus M, Smith DF, Ginsburg V, Blaszczyk M, Mitchell KF, et al. A monosialoganglioside is a monoclonal antibody-defined antigen of colon carcinoma. Science 1981;212:55–6.
21. Nakayama T, Watanabe M, Katsumata T, Teramoto T, Kitajima M. Expression of sialyl Lewis(a) as a new prognostic factor for patients with advanced colorectal carcinoma. Cancer 1995;75:2051–6.
22. Kannagi R. Carbohydrate antigen sialyl Lewisa–its pathophysiological significance and induction mechanism in cancer progression. Chang Gung Med J 2007; 30:189–209.
23. O'Brien DP, Sandanayake NS, Jenkinson C, Gentry-Maharaj A, Apostolidou S, Fourkala EO, et al. Serum CA19–9 is significantly upregulated up to 2 years before diagnosis with pancreatic cancer: implications for early disease detection. Clin Cancer Res 2015;21:622–31.
24. Zhao JG, Hu Y, Liao Q, Niu ZY, Zhao YP. Prognostic significance of SUVmax and serum carbohydrate antigen 19–9 in pancreatic cancer. World J Gastroenterol 2014;20:5875–80.
25. Lefranc MP, Ehrenmann F, Kossida S, Giudicelli V, Duroux P. Use of IMGT® databases and tools for antibody engineering and humanization. Methods Mol Biol 2018;1827:35–69.
26. Metheringham RL, Pudney VA, Gunn B, Towey M, Spendlove I, Durrant LG. Antibodies designed as effective cancer vaccines. mAbs 2009;1:71–85.
27. Chua JX, Vankemmelbeke M, McIntosh RS, Clarke PA, Moss R, Parsons T, et al. Monoclonal antibodies targeting leclex-related glycans with potent antitumor activity. Clin Cancer Res 2015;21:2963–74.
28. Camp RL, Dolled-Filhart M, Rimm DL. X-tile: a new bio-informatics tool for biomarker assessment and outcome-based cut-point optimization. Clin Cancer Res 2004;10:7252–9.
29. Watson NF, Madjd Z, Scrimegour D, Spendlove I, Ellis IO, Scholefield JH, et al. Evidence that the p53 negative/Bcl-2 positive phenotype is an independent indicator of good prognosis in colorectal cancer: a tissue microarray study of 460 patients. World J Surg Oncol 2005;3:47.
30. Duncan TJ, Rolland P, Deen S, Scott IV, Liu DT, Spendlove I, et al. Loss of IFN gamma receptor is an independent prognostic factor in ovarian cancer. Clin Cancer Res 2007;13:4139–45.
31. Abdel-Fatah T, Arora A, Gorguc I, Abbotts R, Beebeejaun S, Storr S, et al. Are DNA repair factors promising biomarkers for personalized therapy in gastric cancer? Antioxid Redox Signal 2013;18:2392–8.
32. Storr SJ, Zaitoun AM, Arora A, Durrant LG, Lobo DN, Madhusudan S, et al. Calpain system protein expression in carcinomas of the pancreas, bile duct and ampulla. BMC Cancer 2012;12:511.
33. Kohls MD, Lappi DA. Mab-ZAP: a tool for evaluating antibody efficacy for use in an immunotoxin. BioTechniques 2000;28:162–5.
34. Koprowski H, Steplewski Z, Mitchell K, Herlyn M, Herlyn D, Fuhrer P. Colorectal carcinoma antigens detected by hybridoma antibodies. Somatic Cell Genet 1979;5:957–71.
35. Zhang Z, Wuhrer M, Holst S. Serum sialylation changes in cancer. Glycoconj J 2018;35:139–60.
36. Nath S, Daneshvar K, Roy LD, Grover P, Kidiyoor A, Mosley L, et al. MUC1 induces drug resistance in pancreatic cancer cells via upregulation of multidrug resistance genes. Oncogenesis 2013;2:e51.
37. Kovtun YV, Audette CA, Mayo MF, Jones GE, Doherty H, Maloney EK, et al. Antibody-maytansinoid conjugates designed to bypass multidrug resistance. Cancer Res 2010;70:2528–37.
38. Partyka K, Maupin KA, Brand RE, Haab BB. Diverse monoclonal antibodies against the CA 19–9 antigen show variation in binding specificity with consequences for clinical interpretation. Proteomics 2012;12:2212–20.
39. Rudnick SI, Adams GP. Affinity and avidity in antibody-based tumor targeting. Cancer Biother Radiopharm 2009;24:155–61.
40. Nakagoe T, Fukushima K, Nanashima A, Sawai T, Tsuji T, Jibiki M, et al. Expression of Lewis(a), sialyl Lewis(a), Lewis(x) and sialyl Lewis(x) antigens as prognostic factors in patients with colorectal cancer. Canadian J Gastroenterol 2000;14:753–60.
41. Weston BW, Hiller KM, Mayben JP, Manousos GA, Bendt KM, Liu R, et al. Expression of human alpha(1,3)fucosyltransferase antisense sequences inhibits selectin-mediated adhesion and liver metastasis of colon carcinoma cells. Cancer Res 1999;59:2127–35.
42. Inagaki Y, Gao J, Song P, Kokudo N, Nakata M, Tang W. Clinicopathological utility of sialoglycoconjugates in diagnosing and treating colorectal cancer. World J Gastroenterol 2014;20:6123–32.
43. Ballehaninna UK, Chamberlain RS. The clinical utility of serum CA 19–9 in the diagnosis, prognosis and management of pancreatic adenocarcinoma: an evidence based appraisal. J Gastrointest Oncol 2012;3:105–19.
44. Lambert JM, Morris CQ. Antibody-drug conjugates (ADCs) for personalized treatment of solid tumors: a review. Adv Ther 2017;34:1015–35.
45. Rios-Doria J, Harper J, Rothstein R, Wetzel L, Chesebrough J, Marrero A, et al. Antibody-drug conjugates bearing pyrrolobenzodiazepine or tubulysin payloads are immunomodulatory and synergize with multiple immunotherapies. Cancer Res 2017;77:2686–98.
46. Zhukovsky EA, Morse RJ, Maus MV. Bispecific antibodies and CARs: generalized immunotherapeutics harnessing T cell redirection. Curr Opin Immunol 2016;40:24–35.
47. Slaga D, Ellerman D, Lombana TN, Vij R, Li J, Hristopoulos M, et al. Avidity-based binding to HER2 results in selective killing of HER2-overexpressing cells by anti-HER2/CD3. Sci Transl Med 2018;10. doi: 10.1126/scitranslmed.aat5775.
48. RodrIguez E, Schetters STT, van Kooyk Y. The tumor glyco-code as a novel immune checkpoint for immunotherapy. Nat Rev Immunol 2018;18:204–11.
49. Langford-Smith A, Day AJ, Bishop PN, Clark SJ. Complementing the sugar code: role of gags and sialic acid in complement regulation. Front Immunol 2015;6:25.
50. Bull C, den Brok MH, Adema GJ. Sweet escape: sialic acids in tumor immune evasion. Biochim Biophys Acta 2014;1846:238–46.
51. Bull C, Boltje TJ, Balneger N, Weischer SM, Wassink M, van Gemst JJ, et al. Sialic acid blockade suppresses tumor growth by enhancing T-cell-mediated tumor immunity. Cancer Res 2018;78:3574–88.

Published OnlineFirst December 23, 2019; DOI: 10.1158/1535-7163.MCT-19-0221

Molecular Cancer Therapeutics

Monoclonal Antibody Targeting Sialyl-di-Lewis^a–Containing Internalizing and Noninternalizing Glycoproteins with Cancer Immunotherapy Development Potential

Silvana T. Tivadar, Richard S. McIntosh, Jia Xin Chua, et al.

Mol Cancer Ther 2020;19:790-801. Published OnlineFirst December 23, 2019.